Computers & Geosciences 82 (2015) 23–30

Contents lists available at ScienceDirect

Computers & Geosciences

journal homepage: www.elsevier.com/locate/cageo

Observations of inertial currents in a lagoon in southeastern Iceland using terrestrial radar interferometry and automated iceberg tracking

Denis Voytenko [a,*], Timothy H. Dixon [a], Mark E. Luther [b], Chad Lembke [b], Ian M. Howat [c], Santiago de la Peña [c]

[a] School of Geosciences, University of South Florida, Tampa, FL, USA
[b] College of Marine Science, University of South Florida, St. Petersburg, FL, USA
[c] School of Earth Sciences and Byrd Polar Research Center, The Ohio State University, Columbus, OH, USA

ARTICLE INFO

Article history:
Received 21 January 2015
Received in revised form
4 May 2015
Accepted 18 May 2015
Available online 19 May 2015

Keywords:
Terrestrial radar interferometry
Iceberg tracking
Inertial currents

ABSTRACT

Warming ocean currents are considered to be a contributing factor to the retreat of marine-terminating glaciers worldwide, but direct observations near the ice–ocean interface are challenging. We use radar intensity imagery and an iceberg tracking algorithm to produce half-hourly current maps within an imaged portion of Jökulsárlón, a proglacial lagoon in southeastern Iceland. Over our 43.5-h observation period, the lagoon has clockwise circulation with current speeds of order 3–8 cm/s and occasional strong glacier outflows of up to ~15 cm/s. The currents driven by the glacial outflows appear to be dominantly inertial.

1. Introduction

1.1. Overview

Sea ice monitoring programs and automated iceberg tracking algorithms have been used in maritime operations to prevent damage to ships or oil rigs (Smith and Banke, 1983). Many of these programs and algorithms involve imaging radar, because of its day/night, all-weather capability. Here we use radar intensity imagery, in conjunction with a new automated iceberg tracking algorithm to develop insights into the hydrography of a proglacial lagoon.

Improved knowledge of ice–ocean interactions is important for predicting the behavior of marine-terminating (tidewater) glaciers, many of which are presently undergoing rapid retreat (Straneo et al., 2013). The role of ocean circulation in melting and calving of marine-terminating glaciers has been recognized for some time (Motyka et al., 2003; Holland et al., 2008; Straneo et al., 2010). However, details of this circulation process in the immediate vicinity of the glacier terminus remain obscure because the possibility of iceberg calving makes direct observation dangerous.

Iceberg motion is an excellent proxy for surface and near-surface currents, since most of the iceberg is submerged, and hence little-affected by winds. GPS receivers have been emplaced on icebergs for current monitoring (Sutherland et al., 2014), but the process is logistically challenging. Rapid remotely-sensed imagery may be useful in fjords and lagoons where iceberg motion can be used to track surface and near-surface currents, and to monitor the frequency and size of glacial outflow events. Here we report results based on imagery acquired with a Terrestrial Radar Interferometer (TRI).

A TRI is a ground-based instrument designed to monitor small-scale displacements on the glacier's surface with high sampling rate and precision using interferometry based on phase comparisons of successive images (Voytenko et al., 2015). However, instead of using phase interferometry to measure the speed of glacier ice, here we exploit the radar intensity imagery and the high sampling rate of the system. Unlike the motion of the glacier ice, smaller icebergs in proglacial lagoons tend to move too fast to be tracked interferometrically, so intensity-based tracking is required.

There are two commonly used methods for detecting motion in imagery: Particle Image Velocimetry (PIV) and Particle Tracking Velocimetry (PTV). PIV is based on measuring the motion of blocks of the image containing numerous particles, while PTV focuses on tracking particles individually. These methods have been extensively studied and applied to a variety of fields including river gauging (Creutin et al., 2003) and iceberg tracking from satellite imagery over long time steps (Silva and Bigg, 2005).

In this study, we focus on a PTV approach for tracking icebergs

* Corresponding author.
E-mail address: dvoytenk@mail.usf.edu (D. Voytenko).

http://dx.doi.org/10.1016/j.cageo.2015.05.012
0098-3004/

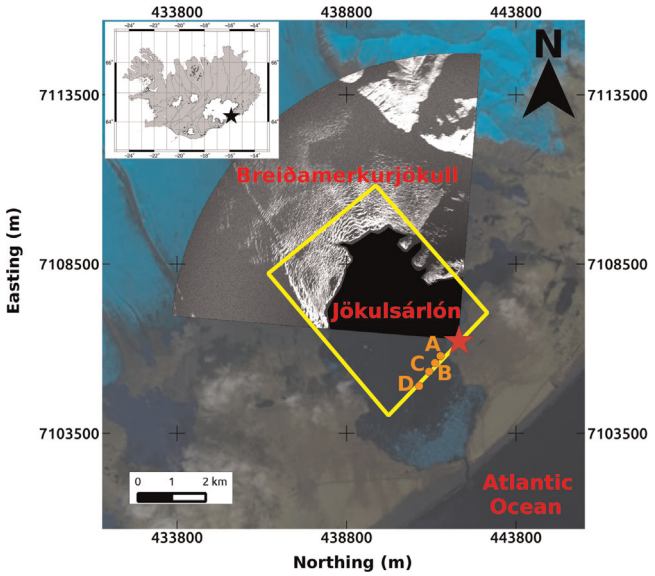

Fig. 1. Study location. The black star in the inset shows the site location in Iceland. The red star shows the location of the radar during the study period. The black and white image shows the area scanned by the radar. The yellow box outlines the lagoon area shown in Figs. 6 and 7. The orange dots represent the BSOP locations over a three-hour period (A is at the beginning of the first hour, B is at the end of the first hour, C is at the end of the second hour, and D is at the end of the third hour). All of the information is overlain on a LANDSAT image obtained from landsatlook.usgs.gov. (For interpretation of the references to color in this figure caption, the reader is referred to the web version of this paper.)

over several minute time steps. First, we use the intensity of the backscattered signal to find the positions of icebergs in the lagoon, whose centroids are detected using a connected component labeling algorithm. Second, we track the iceberg positions in time using a nearest-neighbor approach and generate the resulting velocity maps using radial basis function (RBF) interpolation, a method that has been successfully used for surface, image, and topographic reconstruction (Hardy, 1971; Carr et al., 1997, 2001; Gumerov and Duraiswami, 2007), to infer the behavior of lagoon currents. The iceberg detection and tracking scripts were written in Python using SciPy, NumPy and Matplotlib (Hunter, 2007; Oliphant, 2007) and are available on GitHub along with the TRI intensity images as supplementary materials.

1.2. Site setting

Jökulsárlón is a tidal lagoon at the terminus of Breiðamerkurjökull, an outlet glacier of Vatnajökull, Iceland's largest ice cap (Fig. 1). The lagoon has an area of ~20 km^2, a maximum depth of around 300 m, and is connected to the North Atlantic Ocean via a narrow, engineered, channel (Björnsson, 1996; Björnsson et al., 2001; Howat et al., 2008). Breiðamerkurjökull occasionally calves icebergs into Jökulsárlón. These are the icebergs we track in this study.

The hydrodynamics of this lagoon appear to be complicated, as there are several sources or drivers of potential currents. The lagoon is bounded by mountains on the east and west sides, a glacier on the north side, and the Atlantic Ocean on the south side. The glacier and the ocean bring in strong winds from opposing directions, while ocean tides modulate the currents near the narrow outlet to the ocean. The bounding glacier to the north also subjects the lagoon to calving-driven flows and subglacial drainage.

The lagoon contains both cold, fresh, meltwater from the glacier, and warm, saline, water from the Atlantic Ocean. The salinity and temperature of the lagoon vary seasonally: salinity of 7–17 with temperatures between 1 and 5 °C in the summer (Dixon et al., 2012) and salinity of 15–21 with temperatures between 0.5 and 2 °C in the spring (Brandon et al., 2013). Winter measurements are not available.

2. Methods

2.1. Data acquisition

We used a GAMMA Portable Radar Interferometer (Fig. 2) as the TRI instrument for this study (Werner et al., 2008). This is a Ku-band, real-aperture radar with a range resolution of 0.75 m and an azimuth resolution of 7.5 m at 1 km. The azimuth resolution decreases linearly with distance (e.g., 15 m at 2 km). We deployed the TRI in August of 2012 covering 90-deg arcs with a range of 50 m to 8.5 km and a two minute sampling rate (an ideal sampling rate for measuring rapid iceberg motion in this lagoon), and created 87 half-hour current maps during a continuous 43.5-h observation period.

During the study period, we also deployed an autonomous CTD (conductivity-temperature-depth) profiler, specifically a bottom-stationed ocean profiler (BSOP) (Langebrake et al., 2002) in the lagoon (Fig. 3). During one three-hour period, the BSOP was untethered and moved with the surface currents while continually logging its position (Fig. 1). We used these BSOP position data to verify the current maps and speeds derived from our iceberg tracking algorithm.

2.2. Radar pre-processing

Intensity images are extracted from the radar data and converted to map coordinates with 10 m pixel spacing using the GAMMA software package. The icebergs are detected sequentially image-by-image. Before detection, each image is pre-processed (Fig. 4). The pre-processing is responsible for removing speckle and simplifying iceberg detection. This step is facilitated by the basic characteristics of the radar intensity images. The icebergs act as strong radar scatterers, appearing bright in the image, while the water surface reflects most of the radar energy away from the instrument, and hence appears dark in the image.

The first step in the pre-processing procedure is masking. The mask is the area containing the boundaries of the lagoon, and any pixels outside of the mask are not considered to be an iceberg and

Fig. 2. A typical TRI field set-up. Since the primary purpose of the TRI is to monitor ice surface velocities, the TRI must be set up with a clear view of both the proglacial lake and of the glacier to measure ice surface velocities and to track the icebergs.

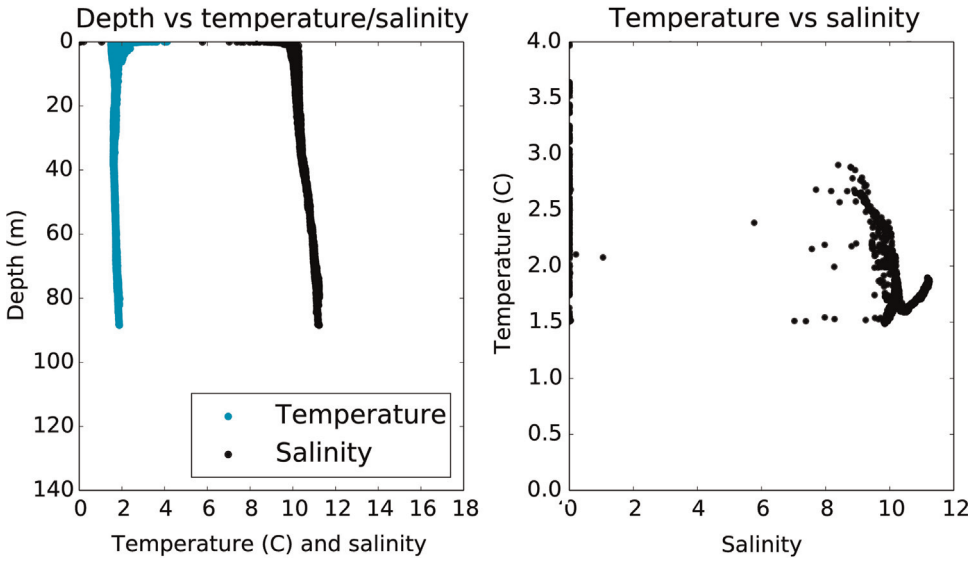

Fig. 3. Salinity, temperature, and depth data from our August, 2012 BSOP deployment (Voytenko et al., 2015). The data show that the lagoon is well mixed at all depths. The great majority of the data lie between salinity of 8–11 and temperatures of 1.5–3 °C.

are discarded. The second step, after the lagoon is selected, focuses on minimizing noise (unfortunately, small icebergs may also be removed in this step). This is accomplished with a sequence of a Gaussian blur ($\sigma=1$), a threshold (0.3), another Gaussian blur ($\sigma=1$) and another threshold (0.3). The thresholding operation creates a binary image, as any pixel value above the threshold criterion is converted to a 1, and every other pixel to a 0. The final image that undergoes iceberg detection is thus a binary image where each pixel is considered either a part of an iceberg (foreground) or a part of the lagoon (background).

2.3. Iceberg detection

Each iceberg in the binary image is detected with a connected component labeling algorithm. The purpose of this algorithm is to identify, and uniquely label, individual components of the image that are only connected to themselves, and distinguish them from other discrete components. We use the SciPy implementation of the two-pass connected component algorithm (scipy.ndimage.measurements.label) based on the classical algorithm proposed by Rosenfeld and Pfaltz (1966).

An illustration of the connected component algorithm is shown in Fig. 5. The image is scanned line-by-line, and border pixels are set to the background value. The first pass over the image labels each pixel in a specific way. If the pixel is a foreground (iceberg) pixel, the algorithm checks to see if any of the four of its neighbors (W, NW, N, NE pixels) are also foreground pixels. Once that check is complete, there are three possibilities (1) if no neighbors are in the foreground, the pixel is given a new label; (2) if only one of the neighboring pixels is in the foreground, then the pixel is given the same label as the other foreground neighbor pixel; (3) if two or more neighboring pixels are in the foreground, then the pixel is assigned a label of either of the foreground neighboring pixels. When this happens, the algorithm stores that all of the labels seen in this step are equivalent. Once all of the pixels have been successfully labeled, the second pass over the image resolves the equivalence between labels: every pixel that belongs to the same set of equivalent pixels is given the same label. Subsequently, all icebergs are relabeled in a consecutive order.

Once every iceberg is given its own label, we find the positions of every pixel with the same label in every iceberg, and calculate the centroid of each iceberg, keeping that information for later tracking. The centroid of an iceberg is the average x and y position of all its constituent pixels, and is compared from image to image for the tracking. The algorithm moves on to the next image, and repeats. Once the centroids for every detected iceberg in every image are found, we begin the tracking process.

2.4. Iceberg tracking

The tracking algorithm is based on a nearest-neighbor approach. The first image initializes the centroids of icebergs

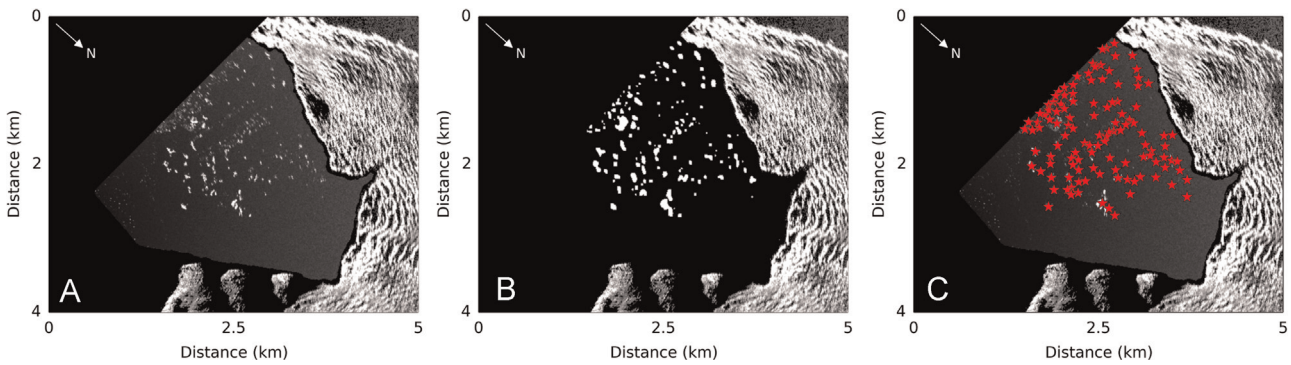

Fig. 4. An example of the pre-processing procedure. The procedure is a sequence of a mask (to get rid of the visible part of the glacier), a Gaussian blur (*sigma*=1), a threshold (0.3), another Gaussian blur (*sigma*=1), and another threshold (0.3). Panel A shows the original image, panel B shows the pre-processed image, and panel C shows the detected iceberg centroids from the pre-processed image.

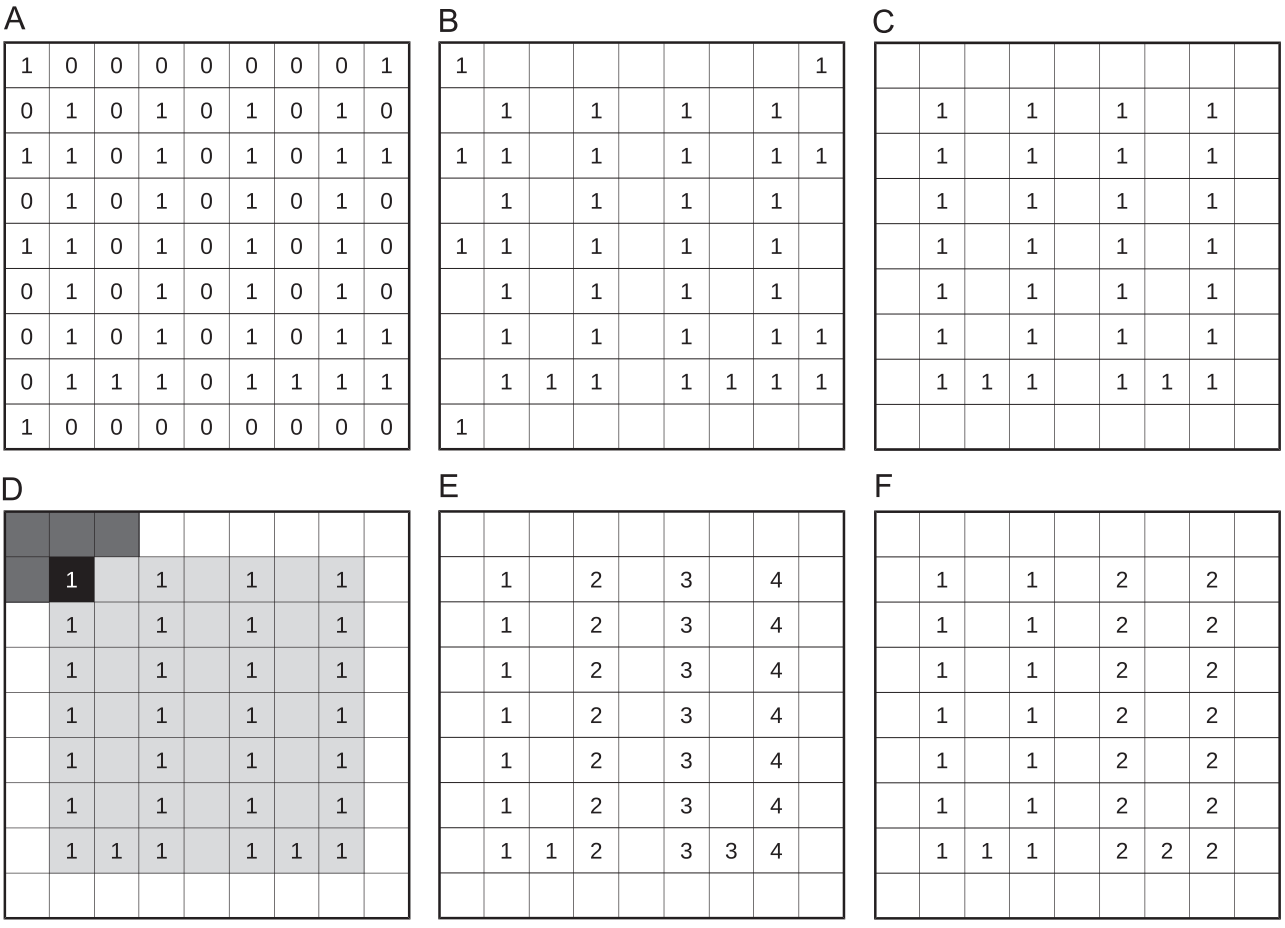

Fig. 5. Step-by-step explanation of the connected component labeling algorithm. (a) Pre-processed binary image. (b) Binary image without visible background pixels. (c) Treat edge pixels as background. (d) Pass 1: check for foreground pixels among the W, NW, N, NE neighbors (dark gray) of every non-edge pixel (light gray) and apply the labeling criteria described in the text. (e) Result after Pass 1 is complete. Note how there are more labels than components. Labels 1 and 2 are equivalent, and so are labels 3 and 4. Each set of equivalent labels belongs to the same component. (f) Pass 2: resolve label equivalences and relabel components sequentially.

detected (these are the icebergs that are going to be tracked). Then, for every new image, the locations of the centroids in the image are compared to the locations of the centroids in the previous image. We specify a maximum distance (20 m for this study) and find the closest centroid in the new image. This is repeated, giving a time series of iceberg centroid positions, which can be converted into velocities. Icebergs that are not detected (e.g., if they become shadowed for one acquisition) are assigned the coordinates from the previous time step.

2.5. Current map generation

Although data are available for every measurement, we linearize the motion over a 30 min time step to account for noise and for temporarily-undetected icebergs. No new icebergs are introduced into the system over this period. Two positions are used to calculate the velocity, one at the beginning (0 min) and one at the end (30 min). Icebergs that moved less than 2 pixels over the half-hour period (speed of 1.1 cm/s), are considered stationary and discarded.

Since we calculate a velocity for every iceberg at every 30-min time step, we specify those velocities at the last known locations of the icebergs. The x and y components of iceberg velocity are interpolated onto a 25x25 grid using a linear radial basis function (RBF) interpolation in SciPy, and each velocity component is interpolated separately.

The RBF interpolation solves for the velocity component at each grid point by using velocity values from every measurement point weighted by the distances to that point. The general equation for the RBF interpolation is (Buhmann, 2003): $s(x) = \sum_{i=1}^{N} \lambda_i \phi(\| p - p_i \|)$, where $s(x)$ is the velocity of the interpolated point, λ_i is a weight coefficient, ϕ is the radial basis function, p is the interpolation point, and p_i is a data point.

Although there are many types of radial basis functions, the linear RBF has a form: $\phi(r) = r$, where r is the radius from the interpolated point to a data point, suggesting that the general interpolation equation is $v(r) = \sum_{j=1}^{N} \lambda_j \phi(r)$, where v is the interpolated velocity, i is an index of an interpolated point, $\phi(r)$ is the RBF, and j is the index of a data point.

Although we have a general equation for the interpolation, we still need to calculate the λ coefficients, which are weights associated with the velocities of the data points and their distances to each other. The λ coefficients are computed by solving a system of linear equations: $\lambda = A^{-1}\mathbf{v}$, where λ is the vector of weights associated with the distances related to the data points, A is a Euclidean Distance Matrix (EDM) describing the distances between points in a specific format, and v is a vector of velocities of the known points. The format of the EDM is

$$\begin{bmatrix} \| p_1 - p_1 \| & \| p_1 - p_2 \| & \cdots & \| p_1 - p_n \| \\ \| p_2 - p_1 \| & \| p_2 - p_2 \| & \cdots & \| p_2 - p_n \| \\ \vdots & \vdots & \ddots & \vdots \\ \| p_n - p_1 \| & \| p_n - p_2 \| & \cdots & \| p_n - p_n \| \end{bmatrix}$$

where p_i is a data point with coordinates (x_i, y_i).

Once we have the coefficients, the velocity at a desired point is

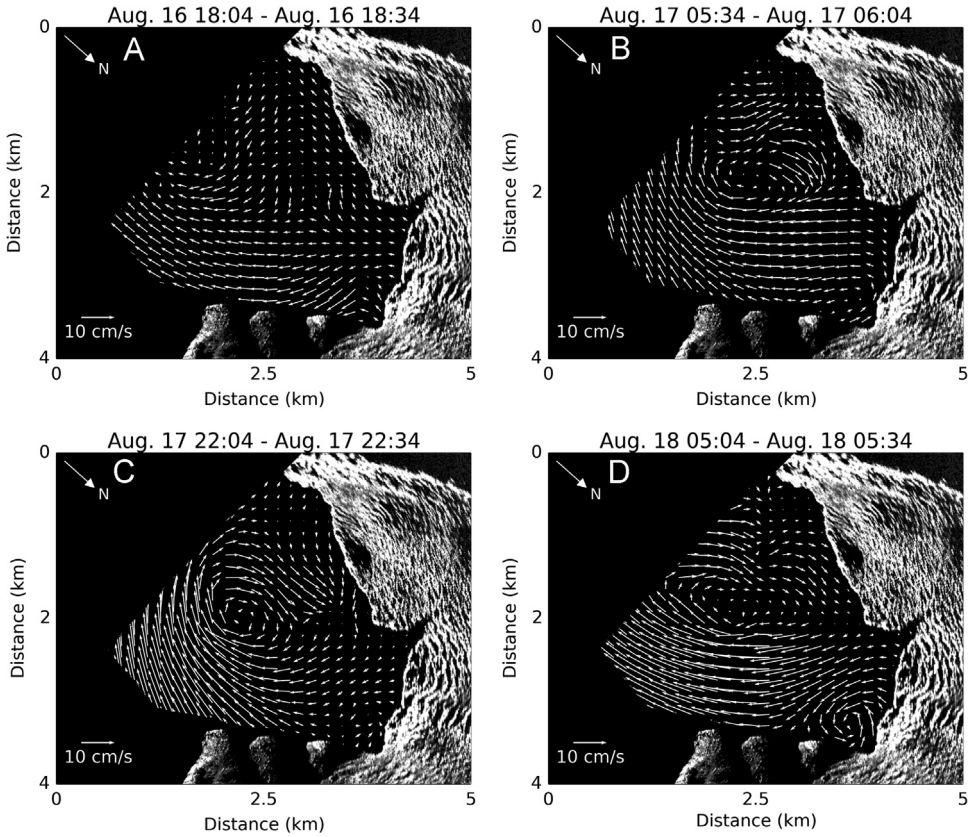

Fig. 6. Iceberg tracking results. Most of the currents are in a clockwise direction and are of order 3–8 cm/s. Panels C and D show faster currents towards the central part of the lagoon, and may reflect outflow events of subglacial water. Strong counterclockwise eddy currents are seen forming in Panel D.

calculated as a function of the distance to all of the available data points, weighted by the calculated coefficients. The components of these interpolated velocities are then represented as arrows on the current maps (Figs. 6 and 7).

2.6. Uncertainty analysis and verification

Uncertainties were estimated using a Monte Carlo simulation with 1000 runs to determine the sensitivity of the linear RBF interpolation method to data noise. We assumed that uncertainties in determining the x and y position of the iceberg centroid were independent, and added a randomly sampled uncertainty parameter (assuming a zero-mean normal distribution and a standard deviation of 1 pixel) to each set of initial and final position measurements, producing 1000 interpolated maps for each of the two components of iceberg motion.

We plot error ellipses related to the measurement uncertainties given a set of x and y position vectors from the Monte Carlo simulation. First, we calculate the covariance matrix

$$\Sigma = \begin{bmatrix} \sigma_x^2 & \sigma_{xy} \\ \sigma_{yx} & \sigma_y^2 \end{bmatrix}.$$

Subsequently, Σ is decomposed into a set of eigenvalues (λ) and eigenvectors (ξ)

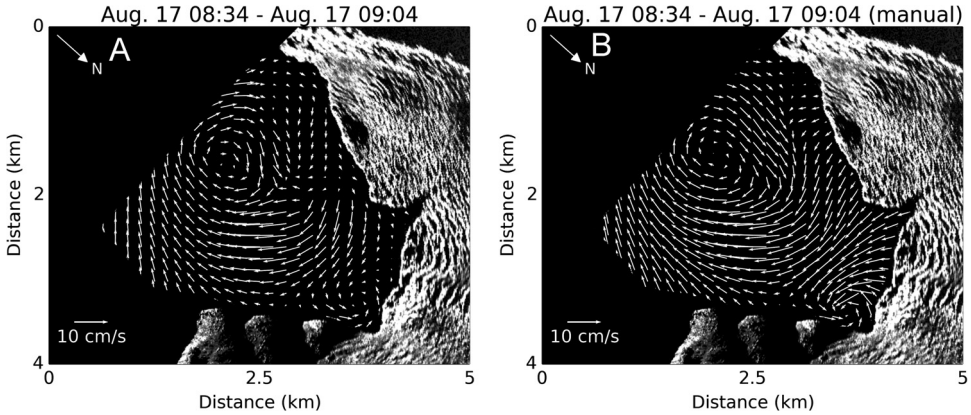

Fig. 7. A comparison between the automatically-detected current map (A) and a current map generated by visually picking (and tracking) the centroids of 15 icebergs at the beginning and the end of the same period (B). Although the pattern and magnitude of the currents are similar in both figures, the automated method appears to smooth out some details (e.g., the magnitude of the eddy current in the bottom left portion of the image and the flow out of the embayment).

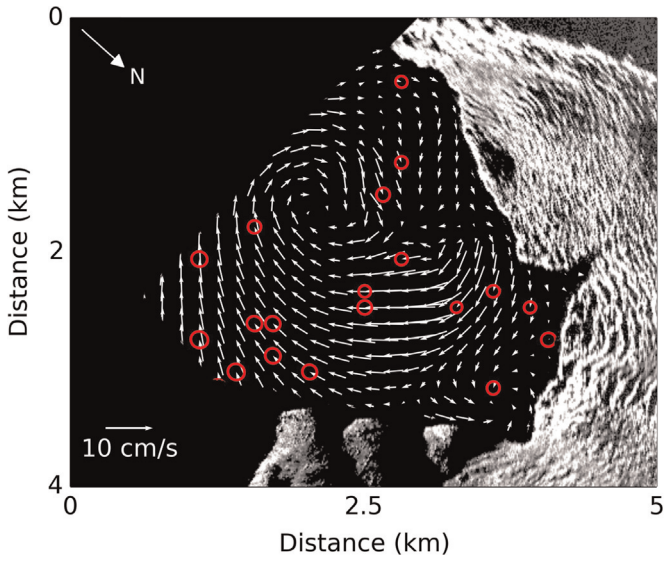

Fig. 8. Error ellipses from the 2012/08/17 08:34–09:04 data for a subset of points derived from the Monte Carlo simulation given a 95 percent confidence interval. Note that most of the ellipses are small compared to the length of the arrows, suggesting that the interpolation method is robust. Also note that the ellipses are bigger in the area (bottom left) with the fewest icebergs seen in the other figures.

$$\lambda = \begin{bmatrix} \lambda_1 \\ \lambda_2 \end{bmatrix}, \quad \xi = \begin{bmatrix} \xi_{11} & \xi_{21} \\ \xi_{12} & \xi_{22} \end{bmatrix}.$$

Then, we follow Haug (2012) to obtain the parametric equations for the error ellipse given a specific confidence interval P_c. For example, we can calculate the area of an ellipse (C^2) that would encompass 95 percent of the data by using the equation: $C^2 = -2\ \ln(1 - P_c)$, and setting $P_c = 0.95$.

Next, we use the square root of this area to scale the ellipse axes, whose length depends on the eigenvalues, and whose orientation depends on the eigenvectors, and θ, a parametric vector on $[0, 2\pi]$. This creates a set of angles, defining points $(x_e(\theta), y_e(\theta))$ to plot the full ellipse around the average x and y positions (Fig. 8)

$$\begin{bmatrix} x_e(\theta) \\ y_e(\theta) \end{bmatrix} = \begin{bmatrix} \hat{x} \\ \hat{y} \end{bmatrix} + \begin{bmatrix} \xi_{11} C\sqrt{\lambda_1}\ \cos(\theta) + \xi_{12} C\sqrt{\lambda_2}\ \sin(\theta) \\ \xi_{21} C\sqrt{\lambda_1}\ \cos(\theta) + \xi_{22} C\sqrt{\lambda_2}\ \sin(\theta) \end{bmatrix}.$$

The Monte Carlo simulation results show the distribution of uncertainties for a subset of selected points in Fig. 8.

The 7–33 percent error in the current speeds (assuming speeds of 3–15 cm/s and a centroid detection error of 1 cm/s) also appears to be reasonable, considering that the TRI was not designed to monitor currents. However, since the visual centroid detection error remains the same regardless of current speeds, the relative uncertainty becomes high in areas with very slow currents (2 cm/s or less).

We verified our technique in two ways: first, by comparing one automatically-detected current map to a manually-detected one; and second, by comparing our estimates to measured motion of the BSOP.

For the first verification method, the manually-detected current map was created by visually identifying the initial and final centroid positions of 15 icebergs over the 30-min period, interpolated the same way as the automated map. The manual iceberg centroid detection produced a current map similar to the automated one (Fig. 7) and had a speed range of 0.14–11 cm/s, while the automatically-detected current map had a speed range of 0.3–11 cm/s.

The second verification method focused on comparisons between different data sets. In this case, the BSOP was transported 1.1 km over a three-hour period, suggesting a surface current velocity of ~10 cm/s (Fig. 1) in a direction consistent with the overall circulation pattern determined by our algorithm. Most of the BSOP is submerged, so its motion should mainly reflect currents rather than winds. The automatically-detected iceberg motion (3–15 cm/s) compares reasonably well with the BSOP motion in both direction and rate (up 11 cm/s in the faster-moving portion of the lagoon) and the manually-detected measurements.

The impact of wind on the current estimates (i.e., the extent to which iceberg motion can be considered a proxy for currents) is addressed in Discussion section.

3. Results

During our 43.5-h study period in 2012, most of Jökulsárlón experienced a clockwise circulation with surface and near-surface current speeds on the order of 3–8 cm/s (Figs. 6 and 7). A video showing current maps and iceberg motion over this 43.5 h period is available in the supplementary materials.

Although the circulation pattern within the lagoon stays fairly constant, the center portion of the lagoon occasionally experiences faster flows (up to ~15 cm/s, Figs. 6 and 7) when there appear to be outflow events from the glacier. We also observe occasional formation of small-scale counter-clockwise eddies near the lagoon shore (Fig. 6).

4. Discussion

The utility of this algorithm is that it can be used in conjunction with high-precision TRI measurements of glacier motion. If a TRI instrument is deployed at a glacier terminating in a lake or fjord, then iceberg motion may be used to infer the surface currents or to observe the frequency and size of glacial outflow events with no additional measurements. Similarly, one or more radars can be used to study iceberg motion in fjords, at lower cost than deploying GPS units on the icebergs (see supplementary information).

One advantage of this method is that it does not directly rely on iceberg cross-section area, shape, or aspect. Instead, it only relies on the iceberg centroid. This is valuable because the rotation of the icebergs changes how they are seen by the radar. Shadow effects due to the nearly-horizontal view angle may cause smaller icebergs to be lost or to appear morphologically different, making it difficult to use feature-based correlation tracking, or to calculate the exact cross-sectional area of the iceberg. However, even if certain parts of an iceberg are shadowed, or if some features of the iceberg are eroded during the filtering step, the centroid should be largely unaffected.

This algorithm can also be modified to detect iceberg calving, as labeling connected components does not depend on motion (we did not attempt this as there were no large calving events during our study period). If the mask for the lagoon is modified to leave a small unmasked band around the terminus, then the only area where the icebergs could be detected is immediately in front of the terminus. Since most of the icebergs float away immediately after calving, and few come close to the ice cliff during circulation, counting the number of icebergs detected in the small area could be used to estimate the number of calving events and to infer the timing of calving.

It is important to keep in mind that this method is sensitive to the spatial density of icebergs. If there are few icebergs in the visible area, the current maps may not be sufficiently detailed (if there are no icebergs in the area, no current measurements can be made). On the other hand, if there are too many icebergs in the visible area, a nearest-neighbor tracking approach may no longer work correctly due to the possibility of overlapping iceberg paths and false connections. Instead, a path predictive algorithm may be needed to account for the possibility of tracking the wrong iceberg

after two icebergs pass close to each other. Of course, for tightly-packed icebergs, motion is inhibited, and current measurements cannot be made with this technique.

For future studies using this method, it may be necessary to adjust the blur and threshold parameters along with the maximum distance between the icebergs to obtain the best results. It would also be beneficial to install an anemometer at the site to resolve issues related to wind-driven iceberg motion (our TRI was not operated in high winds, hence this issue is not important here). Additionally, a tide gauge in the lagoon, combined with a longer observation period, is clearly desirable to assess tidal influences.

Even though both automated and manual detection methods produced similar results of pattern and magnitude (Fig. 7), the automated method appears to smooth out some behavior. The most likely explanation for this is that the automated method used a larger number of icebergs, some of which either moved slower or had substantial changes in illumination (e.g., shadow), which stopped tracking earlier, and smoothed the result. The manual detection method, on the other hand, focused on the 15 most visually-salient icebergs, and may not have accounted for some of the smaller and slower icebergs, while also allowing us to pick iceberg positions by eye and ignore any potential variability in illumination.

We can learn more about the period of fast circulation (August 17–18, 2012) by either tracking a single iceberg (Figs. 9 and 10) or by averaging a number of the images from this time period and plotting them (Fig. 11). During this period, the current exhibits elliptical circulation with long axis of approximately 1300 m and short axis of approximately 900 m, while it takes an iceberg approximately 12–15 h to complete a full loop (see supplementary materials for video).

Although currents in a lagoon are driven by some combination of tides, winds, and any additional externally-forced inflow or outflow events, our analysis of iceberg trajectory geometry suggests that currents in the lagoon mainly reflect inertial forces. Inertial motion describes the circular behavior of icebergs subject to a burst of applied force (e.g., glacial outflow or wind) and the subsequent impact of the Coriolis effect on their trajectories. Since the motion is clockwise, the expected direction of Coriolis motion in the Northern Hemisphere, and since the circular motion of the icebergs becomes dominant after visible outflows, the driver for inertial motion is likely strong glacier meltwater outflow events (see animated figure in the supplementary materials).

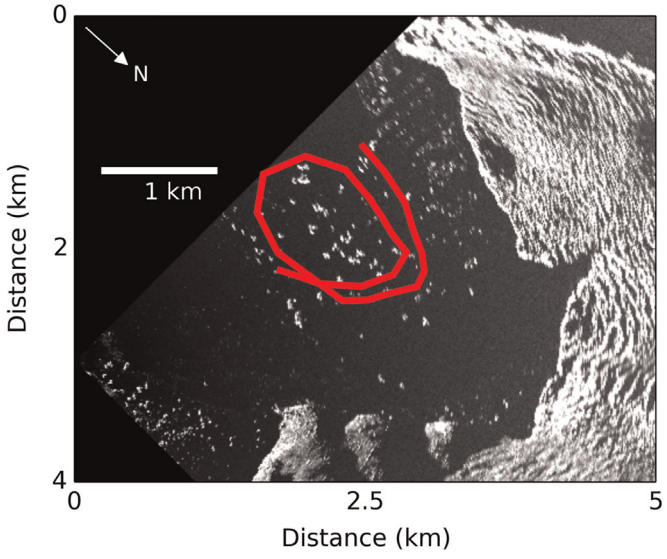

Fig. 9. Path of a single, manually-detected, iceberg over a 23 h period (August 17, 13:00 to August 18, 12:00). The period and dimensions of this circulation pattern are consistent with those for inertial motion at this latitude.

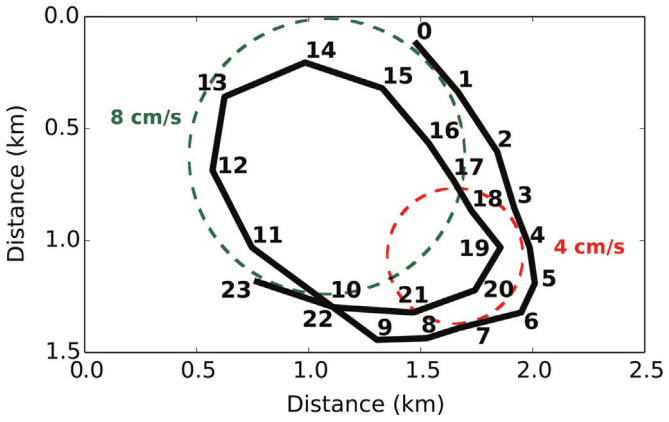

Fig. 10. Position-time plot of a track of a single iceberg shown in Fig. 9. The data are shown at hourly intervals. Hour 0 is August 17, 13:00. The velocities range between 4 and 11 cm/s. Note that the iceberg velocity decreases as it gets closer to the glacier front. The figure also shows theoretical inertial radii, which are calculated for a speed of 4 cm/s (300 m radius, 600 m diameter, red) and 8 cm/s (600 m radius, 1200 m diameter, green). The similarity of the theoretical calculations to the measured iceberg path supports the hypothesis that post-outflow currents are dominated by inertial motion. (For interpretation of the references to color in this figure caption, the reader is referred to the web version of this paper.)

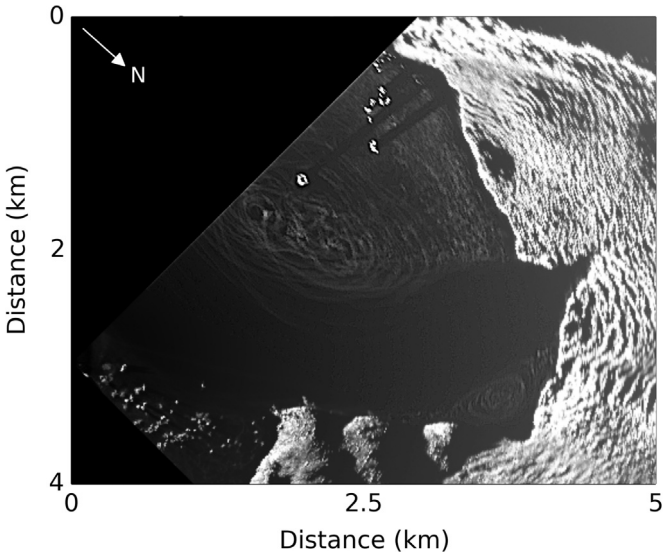

Fig. 11. Averaged image from the intensity data on August 18th (currents sharpened for clarity). Note the strong elliptical pattern of circulation and its dimensions (width of ~900 m and length of ~1300 m; see also Figs. 9 and 10). This pattern may reflect iceberg motion subject to inertial effects after an outflow event. Also note that a few very large icebergs were motionless (and therefore grounded – note radar shadow) during this period. This suggests that iceberg motion may contribute to the mixing of lagoon waters.

The circulation from the observed iceberg motion can be compared to theoretical calculations for inertial currents. The Coriolis parameter, f, is $f = 2\Omega \sin \phi$, where Ω is the rotational rate of the Earth (7.292E−5 rad/s) and ϕ is latitude (64°N at our study site, giving f=1.31E−4).

The Coriolis parameter can be used to calculate how long it would take an iceberg to complete one full loop (inertial period) of a specific inertial radius. The inertial period, T, is given by $T = 2\pi/f$, and is 13.3 h at the latitude of Jökulsárlón, in approximate agreement with observations. The inertial radius, r, is $r = V/f$, where V is the velocity of the current.

The speed variations may explain the pattern of circulation, in particular its “teardrop” shape. For a purely inertial current, the inertial radius at a given latitude depends only on current speed. For a speed of 4 cm/s, the radius is 300 m, while a speed of 8 cm/s

generates a radius of 600 m (Fig. 10). This is in approximate agreement with observations shown in Figs. 9 and 10 and supports the hypothesis that iceberg circulation within a portion of the lagoon during our observation period is essentially inertial motion, likely caused by bursts of subglacial drainage.

The shape of the current track may also be influenced by the relationship between the glacier terminus and the moraine deposits (shown at the bottom of the intensity images; Fig. 9). Since the glacier terminus changes position and shape, and the moraine deposits do not, there may be a dynamic feedback mechanism between the orientation of circulation and the terminus position. As the terminus position changes, the direction of subglacial outflows may vary as well, forcing the outflows to change direction at the stationary moraine boundary. This process may impact the circulation pattern, and may subsequently impact the terminus morphology at times when warm water intrusion becomes important (e.g., spring).

Fig. 11 shows several "stranded icebergs" marked by strong radar returns from the front of the icebergs, and shadowing behind, over the ~12 h observation period. These icebergs are so large that they become grounded on the lagoon bottom. This implies that the range of iceberg depths is sufficient that iceberg motion acts to stir the lagoon water, which may be a contributing factor (along with long-term wind-driven circulation) to the lagoon mixing, explaining the limited range of salinity and temperature (Fig. 3) during summer conditions.

Although we did not have an anemometer at the site and we only operated the TRI during low wind conditions due to operational limitations associated with the large antennas, we can speculate on the effects of wind-driven motion on our measurements. Ekman (1905) derived a simple empirical formula, $V_0 = 0.0127\, h(\sin\ \phi)^{-1/2}$, to estimate surface current speed (V_0) given a wind speed (h) and latitude (ϕ). This approach assumes that motion is considered over a few inertial periods (Stewart, 2004), and includes Ekman's assumptions of infinite water depth and no lateral boundaries, which are not strictly valid here. At the latitude of the lagoon (64°N), assuming a light breeze (2.5 m/s) suggests a surface current speed of 0.033 m/s (3.3 cm/s). Assuming a strong breeze (12 m/s, a speed at which operating the TRI is challenging) suggests a surface current speed of 0.16 m/s (16 cm/s). If we assume a constant light breeze at the study site, some of the measured current velocities could reflect wind-driven circulation.

5. Conclusions

TRI measurements of glaciers can be used not only to study glacier motion, but also to study surface and near-surface currents in glacial lakes or fjords and to monitor glacial outflow events, assuming trackable objects such as icebergs are visible in the radar imagery. Current motion can be determined without any extra data collection efforts and with straightforward post-processing.

TRI intensity images have been used to produce lagoon current maps with 30-min sampling intervals, showing the variability of current motion within Jökulsárlón, a proglacial lagoon in Iceland. During our study, currents have typical speeds of 3–8 cm/s and follow a clockwise rotation, with occasional bursts of outflow along the center portion of the lagoon that are likely related to subglacial drainage. These outflow events appear to set up patterns of inertial circulation.

Acknowledgments

We thank the Jökulsárlón lagoon staff for their help with data collection. We also thank Björn Oddsson for his assistance with logistics in the field. D.V. and T.H.D. received support from NASA grants and start-up funds from USF. We thank two anonymous reviewers for their valuable comments which helped improve the manuscript.

Appendix A. Supplementary data

Supplementary data associated with this article can be found in the online version at http://dx.doi.org/10.1016/j.cageo.2015.05.012.

References

Björnsson, H., 1996. Scales and rates of glacial sediment removal: a 20 km long and 300 m deep trench created beneath Breiðamerkurjökull during the Little Ice Age. Ann. Glaciol. 22, 141–146.
Björnsson, H., Pálsson, F., Guðmundsson, S., 2001. Jökulsárlón at Breiðamerkursandur, Vatnajökull, Iceland: 20th century changes and future outlook. Jökull 50, 1–18.
Brandon, M., Hodgkins, R., Björnsson, H., Ólaffson, J., 2013. Hydrographic measurements in Jökulsárlón lagoon, Iceland. In: American Geophysical Union Fall Meeting. San Francisco, CA, USA, pp. 9–13.
Buhmann, M.D., 2003. Radial Basis Functions: Theory and Implementations, vol. 5. Cambridge University Press, Cambridge.
Carr, J.C., Beatson, R.K., Cherrie, J.B., Mitchell, T.J., Fright, W.R., McCallum, B.C., Evans, T.R., 2001. Reconstruction and representation of 3D objects with radial basis functions. In: Proceedings of the 28th Annual Conference on Computer Graphics and Interactive Techniques, ACM, New York, NY, USA, pp. 67–76.
Carr, J.C., Fright, W., Beatson, R.K., 1997. Surface interpolation with radial basis functions for medical imaging. IEEE Trans. Med. Imaging 16, 96–107.
Creutin, J., Muste, M., Bradley, A., Kim, S., Kruger, A., 2003. River gauging using PIV techniques: a proof of concept experiment on the Iowa River. J. Hydrol. 277, 182–194.
Dixon, T.H., Voytenko, D., Lembke, C., de la Peña, S., Howat, I., Gourmelen, N., Werner, C., Oddsson, B., 2012. Emerging technology monitors ice-sea interface at outlet glaciers. Eos, Trans. Am. Geophys. Union 93, 497–498.
Ekman, V.W., 1905. On the influence of the earth's rotation on ocean currents. Ark. Mat. Astron. Fys. 2, 1–53.
Gumerov, N.A., Duraiswami, R., 2007. Fast radial basis function interpolation via preconditioned Krylov iteration. SIAM J. Sci. Comput. 29, 1876–1899.
Hardy, R.L., 1971. Multiquadric equations of topography and other irregular surfaces. J. Geophys. Res. 76, 1905–1915.
Haug, A.J., 2012. Bayesian Estimation and Tracking: A Practical Guide. John Wiley & Sons, Hoboken, NJ, USA.
Holland, D.M., Thomas, R.H., DeYoung, B., Ribergaard, M.H., Lyberth, B., 2008. Acceleration of Jakobshavn Isbrae triggered by warm subsurface ocean waters. Nat. Geosci. 1, 659–664.
Howat, I.M., Tulaczyk, S., Waddington, E., Björnsson, H., 2008. Dynamic controls on glacier basal motion inferred from surface ice motion. J. Geophys. Res.: Earth Surf. 2003–2012 113.
Hunter, J.D., 2007. Matplotlib: a 2D graphics environment. Comput. Sci. Eng. 9 0090-95.
Langebrake, L.C., Lembke, C.E., Weisberg, R.H., Byrne, R.H., Russell, D.R., Tilbury, G., Carr, R., 2002. Design and initial results of a bottom stationing ocean profiler. In: OCEANS'02 MTS/IEEE, vol. 1, IEEE, pp. 98–103.
Motyka, R.J., Hunter, L., Echelmeyer, K.A., Connor, C., 2003. Submarine melting at the terminus of a temperate tidewater glacier, LeConte Glacier, Alaska, USA. Ann. Glaciol. 36, 57–65.
Oliphant, T.E., 2007. Python for scientific computing. Comput. Sci. Eng. 9, 10–20.
Rosenfeld, A., Pfaltz, J.L., 1966. Sequential operations in digital picture processing. J. ACM (JACM) 13, 471–494.
Silva, T.A., Bigg, G.R., 2005. Computer-based identification and tracking of Antarctic icebergs in SAR images. Remote Sens. Environ. 94, 287–297.
Smith, S.D., Banke, E.G., 1983. The influence of winds, currents and towing forces on the drift of icebergs. Cold Reg. Sci. Technol. 6, 241–255.
Stewart, R.H., 2004. Introduction to Physical Oceanography. Texas A & M University http://oceanworld.tamu.edu/home/course_book.htm.
Straneo, F., Hamilton, G.S., Sutherland, D.A., Stearns, L.A., Davidson, F., Hammill, M. O., Stenson, G.B., Rosing-Asvid, A., 2010. Rapid circulation of warm subtropical waters in a major glacial fjord in East Greenland. Nat. Geosci. 3, 182–186.
Straneo, F., Heimbach, P., Sergienko, O., Hamilton, G., Catania, G., Griffies, S., Hallberg, R., Jenkins, A., Joughin, I., Motyka, R., et al., 2013. Challenges to understand the dynamic response of Greenland's marine terminating glaciers to oceanic and atmospheric forcing. Bull. Am. Meteorol. Soc. 94.
Sutherland, D.A., Roth, G.E., Hamilton, G.S., Mernild, S.H., Stearns, L.A., Straneo, F., 2014. Quantifying flow regimes in a Greenland glacial fjord using iceberg drifters. Geophys. Res. Lett. 41, 8411–8420.
Voytenko, D., Dixon, T.H., Howat, I.M., Gourmelen, N., Lembke, C., Werner, C.L., de la Peña, S., Oddsson, B., 2015. Multi-year observations of Breiðamerkurjökull, a marine-terminating glacier in southeastern Iceland, using terrestrial radar interferometry. J. Glaciol. 61, 42–54.
Werner, C., Strozzi, T., Wiesmann, A., Wegmuller, U., 2008. A real-aperture radar for ground-based differential interferometry. In: IEEE International Symposium on Geoscience and Remote Sensing, 2008, IGARSS 2008, vol. 3, IEEE, pp. III-210.